iScience

CellPress
OPEN ACCESS

Article

Lidar as a potential tool for monitoring migratory insects

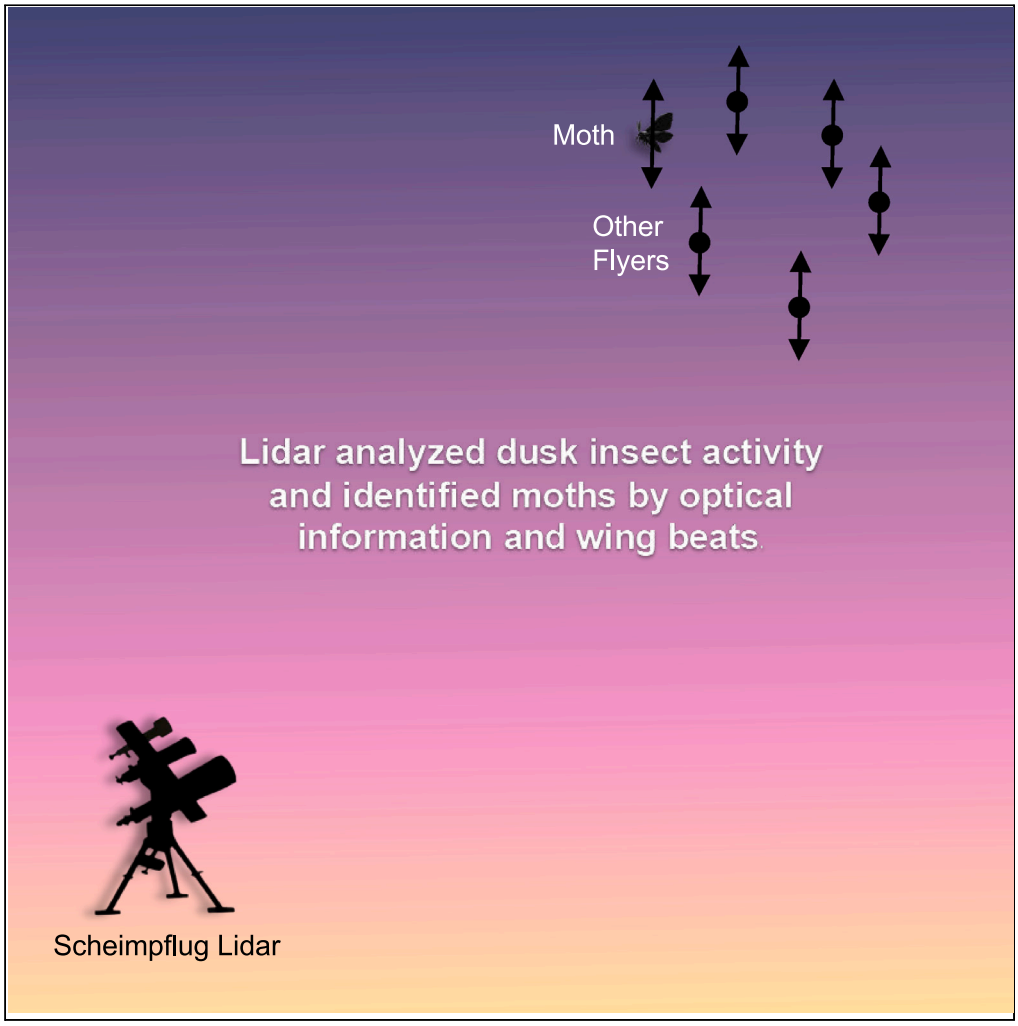

Hui Chen, Meng Li, Hampus Månefjord, ..., Gao Hu, Eric Warrant, Mikkel Brydegaard

hui.chen@njau.edu.cn (H.C.)
meng.li@fysik.lu.se (M.L.)
mikkel.brydegaard@fysik.lu.se (M.B.)

Highlights

Lidar to elucidate the low-height dusk movements and detailed information of insects

Moths were filtered based on optical information and wing beat frequency by lidar

Chen et al., iScience 27, 109588
May 17, 2024
https://doi.org/10.1016/j.isci.2024.109588

iScience

CellPress
OPEN ACCESS

Article

Lidar as a potential tool for monitoring migratory insects

Hui Chen,[1,4,10,*] Meng Li,[2,10,*] Hampus Månefjord,[2] Paul Travers,[3] Jacobo Salvador,[2] Lauro Müller,[2] David Dreyer,[4] Jamie Alison,[6] Toke T. Høye,[6,7] Gao Hu,[1] Eric Warrant,[4] and Mikkel Brydegaard[2,5,8,9,11,*]

SUMMARY

The seasonal migrations of insects involve a substantial displacement of biomass with significant ecological and economic consequences for regions of departure and arrival. Remote sensors have played a pivotal role in revealing the magnitude and general direction of bioflows above 150 m. Nevertheless, the takeoff and descent activity of insects below this height is poorly understood. Our lidar observations elucidate the low-height dusk movements and detailed information of insects in southern Sweden from May to July, during the yearly northward migration period. Importantly, by filtering out moths from other insects based on optical information and wingbeat frequency, we have introduced a promising new method to monitor the flight activities of nocturnal moths near the ground, many of which participate in migration through the area. Lidar thus holds the potential to enhance the scientific understanding of insect migratory behavior and improve pest control strategies.

INTRODUCTION

Insect migrations displace vast quantities of individuals, biomass, and nutrients across the earth's surface, with profound implications for both agriculture and biodiversity.[1–3] Transitioning to the nocturnal aspect, the night sky is a less explored avenue in insect migration studies. The cover of darkness offers a different set of environmental conditions and challenges, prompting distinct behavioral adaptations among migrating insects. Most of the large nocturnal migrants are moths,[4] which commonly migrate at significant heights above the ground (as high as 1 km), taking advantage of seasonally favorable winds.[5] Many migratory moth species provide beneficial ecosystem functions, such as pollination,[6] but many are also economically significant pests or vectors of plant-disease viruses.[7–9] The detection, quantification, and characterization of moth migratory movements are therefore of great value to insect ecologists and ethologists for improving our understanding of the drivers and consequences of migration.

A major challenge in insect migration research is to understand where and when migrating insects take off and descend.[10,11] This is particularly crucial to aid agriculturists in predicting the timing and location of migration events, helping to mitigate damaging pest outbreaks.[12,13] Vertical-looking entomological radar (VLR) has proven pivotal for producing accurate estimates of both the horizontal and vertical components of the flight vectors of target insects at heights above roughly 150 m,[4,14,15] but its inherent noise interference below 150 m has prohibited the study of insect migration close to the ground.[11,16–19] Scanning radar can detect the targets by adopting different angles with scanning mode, which has been utilized for monitoring the agricultural pest[9]; it hardly provides flight detailed information of migratory insects. While frequency-modulated continuous-wave (FMCW) radar has demonstrated its capability to surmount inherent noise challenges, thereby presenting itself as a promising tool for monitoring insect migrants,[20–22] its practical application in field monitoring of migratory insects has not been realized to date. Furthermore, while harmonic radar can detect low-altitude insect migratory behavior with high-resolution positional data, the need for tagging renders this method unsuitable for the comprehensive monitoring of migratory insects. Building upon previous work, entomological lidar (laser radar[23]), with lower inherent noise interference, can be further employed and is an extra option for efficient insect monitoring below 150 m for both tagged[24] and untagged[25] insects, potentially unraveling the remaining mysteries of insect migration at low heights.[25]

[1]Department of Entomology, Nanjing Agricultural University, Nanjing 210095, China
[2]Department Physics, Lund University, Sölvegatan 14c, 22363 Lund, Sweden
[3]Department Biological Engineering, Polytech Clermont, 2 Av. Blaise Pascal, 63100 Aubière, France
[4]Lund Vision Group, Department Of Biology, Lund University, Sölvegatan 35, 22362 Lund, Sweden
[5]Department Biology, Lund University, Sölvegatan 35, 22362 Lund, Sweden
[6]Department Ecoscience, Aarhus University, C. F. Møllers Allé 8, 8000 Aarhus C, Denmark
[7]Arctic Research Centre, Aarhus University, Ole Worms Allé 1, 8000 Aarhus C, Denmark
[8]FaunaPhotonics, Støberigade 14, 2450 Copenhagen, Denmark
[9]Norsk Elektro Optikk, Østensjøveien 34, 0667 Oslo, Norway
[10]These authors contributed equally
[11]Lead contact
*Correspondence: hui.chen@njau.edu.cn (H.C.), meng.li@fysik.lu.se (M.L.), mikkel.brydegaard@fysik.lu.se (M.B.)
https://doi.org/10.1016/j.isci.2024.109588

Extending existing applications of Lidar, it has been successfully applied in different kinds of insect monitoring with the advantage of detection sensitivity and specificity.[26–28] Such specificity can be achieved with multiband lidars that can quantify molecular absorption by melanin,[29] nanoscopic wing thicknesses,[30] or microstructural information such as surface roughness.[29] The widely diverse detection distances and the rapid movements of free-flying insects pose challenges to focusing and classification of insect species.[31] However, wing interference phenomena and wingbeat modulation are unaffected by focus blur and show potential for insect classification based on lidar observations.[26,28,32–34] Lidar may also provide an accurate description of flight parameters, such as flight velocity and speed, which are scarcely documented for moths. This lack of documentation hinders understanding of moth migration and hampers the development of effective conservation and pest control strategies.

In this study, we further explore the utility of lidar for insect surveillance at low heights by collecting real-time, *in situ*, spatially profiled observations during two months of the insect migration season. The study was conducted in a rural area in southern Sweden within a healthy ecosystem (including pasture, forests, and wetlands) with minimal light pollution. Southern Sweden is positioned along the migratory path from southern Europe to the Scandinavian Peninsula and serves as a vital stopover for migratory insects.[2,35] During the northward migration period from May to July, nightly migratory insect takeoff and landing behaviors occur in this region.[2,35]We used lidar to derive flight parameters for moths and other insects, such as vertical velocity and height, recorded around dusk when migration activity normally begins. Moreover, through the optical information and wing beat captured by our refined lidar methods, we have demonstrated in this paper the potential to distinguish moth signals from those of other insects. Our study enhances the methodology for insect surveillance and, by distinguishing moths, lays the groundwork for deeper analysis of migratory moth activity patterns. Our pioneering research introduces a promising tool for remote monitoring, poised to significantly contribute to the development of innovative and more effective conservation and pest control strategies.

RESULTS

Our field campaign was executed at Stensoffa Field Station (55°41′44″N 13°26′50″E) between 25th May and 21st July, 2022. The operation of the lidar system was conditional on favorable atmospheric conditions, specifically excluding instances of rain and strong winds. The schedule for data recording varied. Full-day recording was executed on certain days, whereas, on others, recording was constrained to a time window from 18:00 to 24:00 (sunset occurred between 20:52 and 21:21 during the measurement period). Our results are later controlled for observation hours.

The lidar system was oriented northwards (Figures 1A and 1B) and aimed skyward with an elevation angle of 30° (Figure 1C). Although the Scheimpflug lidar operates to infinity, the furthest insect in this study was detected at roughly 700 m distance, corresponding to a height of 400 m. In our previous study[32] the lidar transect was conducted at ground level, closer to vegetation where insects emerge and are more abundant, achieving a detection range of up to ∼2 km. However, the lidar's 30° elevation angle and near limit of 35 m (approximately 18 m in height) restrict observations to above 18 m. The experimental site's lack of tall trees and average tree height (15–20 m, based on Global Ecosystem Dynamics Investigation tree height maps) support the assumption that the observed signals are not from plant debris or plankton. See Figure 1 for an image of the surrounding vegetation.

The lidar system was oriented skyward to observe insect migration at elevated altitudes. Given the anticipated lower insect density at heights hundreds of meters above the ground, the furthest detection at 400 m elevation is within expectations. The 30° elevation angle was chosen over a vertical (zenith) configuration for two reasons: firstly, to attempt to prolong the transit time of insects through the lidar beam, thereby facilitating better data capture, and, secondly, to permit housing the instrument within a protective garage tent (Figures 1A and 1B), thereby reducing the need for constant supervision. At a 30° elevation, the lidar's trajectory passed above varied vegetation, including an assortment of tree species (Figure 1D). Throughout the campaign, we gathered lidar data for a total of 18 days, yielding 17,254 insect observations.

Our lidar measurements recorded insect activity patterns with high spatial and temporal resolution throughout the day and at various heights (Figure 2). It is pertinent to note that the alignment of the beam and receiver, which first intersect at a height of 20 m above the ground, substantially reduces the chances of detecting dispersal flights emanating from the vegetation below. Our observations demonstrate prominent insect activity during the late afternoon and evening hours (until around just before midnight), in contrast to a significantly reduced activity observed from then until just after sunrise. Insect activity again peaks around mid-morning before declining later in the morning and during the early afternoon. The campaign was conducted in the south of Sweden, with short summer nights close to midsummer, typically experiencing sunrise as early as 04:21 and sunset nearing 21:54, on average (there is 17:30 h of daylight; 19:30 h also include twilight, and light levels exceed astronomical twilight limits throughout the day (https://www.timeanddate.com/sun/).

Interestingly, despite the lengthy daylight periods, most insect activity at higher heights (over 100 m) was observed during the late afternoon and evening, with most observations made after 21:00 and before midnight. This might be due to the fact that crepuscular or nocturnal insects are typically more tolerant to colder temperatures, which are commonly experienced during the night and at higher altitudes. The notable decrease in activity at altitudes above approximately 50 m just before midnight could be attributed to high-altitude insects, potentially migratory ones, having landed by this time.

By implementing a previously described method[36] (see also quantification and statistical analysis), we determined the velocities of observed insects, as well as their vertical movement directions and speeds (that is, whether they were ascending or descending). This could be achieved by initially setting the lidar system at a vertical beamline position and then tilting the system to a 30° elevation angle. (Figure 1A).

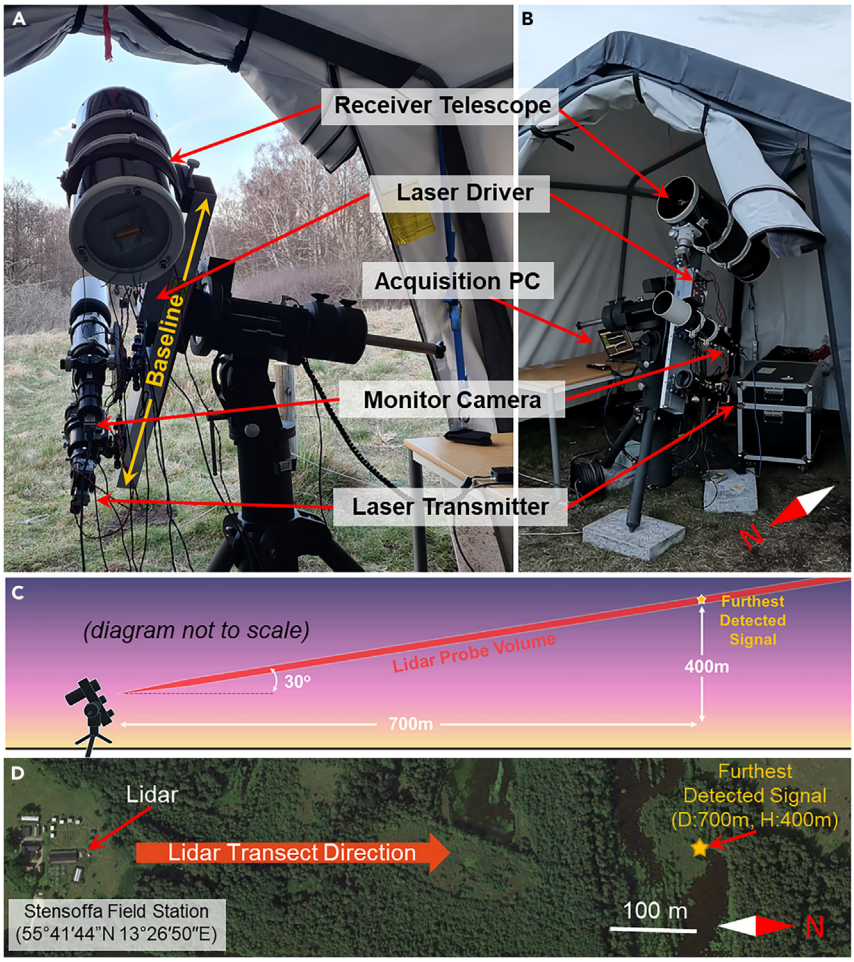

Figure 1. The experimental setting at Stensoffa ecological field station, southern Sweden, in 2022

(A–C) The lidar instrument setup with 30° elevation angle, optimized to observe migratory insect patterns.

(D) A satellite image pinpointing the location of the experimental site.

The same method was previously employed by another group using a horizontal baseline that yielded lateral east-west movements.[36] Ranging uncertainty in Scheimpflug lidar arises from the beam beam width.[37] This uncertainty is approximately 3%–5% of the range but also allows to estimate size[26] and coarse assessment of transverse velocity.[36]

Previous radar studies have demonstrated evening ascents and descents,[11] and studies on foraging insects using quadrant photodiodes concluded that movement was predominantly lateral during the day and close to the ground.[38] Figure 3A shows the total movement direction and speed of all detected insects over an entire day or summed across all insect sizes and detectable heights. Insect size was approximated using apparent size, which is derived from the pixel footprint from the camera and telescope magnification, providing an estimate of the insect's dimensions (this calculation is presented in the STAR methods section). It is crucial to underscore that the apparent size of an insect is fundamentally a representation of its projection onto the camera sensor. This measurement can be markedly influenced by the insect's body orientation during flight: when an insect is projected sideways compared to a projection from its posterior or anterior onto the camera sensor, the apparent size is observed to be larger from the sideways projection. The variation in apparent size can be noticeable, depending on the angle or position of the insect. Therefore, while the apparent size data offer a close estimate, it may not always directly reflect the precise physical dimensions of an insect.

By sub-sectioning the data into different height intervals (Figures 3A–3D), we noticed a decrease with height in the number of observations and a shift in the overall movement direction from predominantly upward (ascending) to equally upward and downward (descending). Similar patterns were noted in Figures 3E–3H: as for late hours, movement became more even in both directions. Moreover, insects with smaller size estimates, such as those under 10 mm, typically exhibit relatively slower movement speeds, and the central tendency (median) is at zero for heading direction (Figures 3A and 3I–3L). As the size increases, larger insects seem to trend toward an upward heading and demonstrate increased flight speeds. When we examine insects of larger proportions, specifically those exceeding 40 mm, these occasionally exhibit higher speeds, yet their overall heading distribution appears to be evenly divided between ascending and descending individuals. There

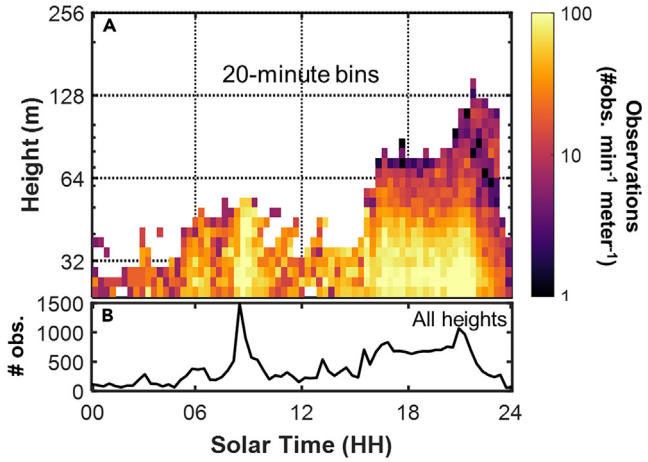

Figure 2. Diel insect variation over the course of 18 days, all types of insects are included

(A) Insect activity across various heights throughout the day, which was compensated for observation hours for a period of 18 days.

(B) Overall number of detected flights regardless of height. All insect activity data have been post-compensated to correct for biases due to inconsistencies in observational hours.

was a strong tendency for insects to ascend rather than descend (Figure 3A), suggesting that our study area was a strong population source[39] for many insect species during data collection.

Additionally, two distinct patterns of change were observed. One pattern indicates that the central tendency shifts from upwards to no directional change with increasing height and hour after sunset. The other pattern reveals the disappearance of the bimodal distribution. This latter observation implies that there is an increasing randomness in the directions of the insects as the night progresses and at higher altitudes, whereas, around dusk and at lower heights, insects predominantly move either up or down. This observation further complements the findings of the study, reinforcing the notion that the movement patterns of insects vary significantly based on the time of day and their altitude.

These findings offer the potential for future advancements in monitoring the ascending and descending behaviors of migratory insects, as well as studies related to predation, such as between birds, bats, and insects. Such studies would significantly benefit from the ability to accurately distinguish migratory moth signals from those of other insects. If such a distinction could be made, we can delve deeper into understanding the intricacies of moth behavior and their contribution to overall insect ecology.

Finally, we showcase an instance (Figure 4) where we successfully singled out a moth observation from those of other insects, an accomplishment achieved due to a long transit time and wing stroke signal. This observation, however, does not typify the majority of our recorded data in this study. To increase our chances of such successful identifications, we attempted to extend the transit time by reducing the lidar beam's elevation angles. Unfortunately, this approach proved insufficient as most observations remained too short to accurately identify wing beats and wing strokes. Despite this challenge, we can nonetheless demonstrate, with a clear capture of wing strokes, that we can indeed distinguish moths from other insects according to moth's high wing depolarization ratios. In Figure 4A, we offer an illustrative example of a lidar signal: the flight trajectory of a moth at an elevated height. Here, the distance can be inferred from the absolute pixel numbers and the heading and sizing can be inferred from the differential pixel numbers. The camera exposures over time represent the passage of time, and the false color scheme is indicative of light intensity and its polarization state. In the generated false color image, specific light characteristics are mapped to distinct RGB color layers: depolarized light intensity is encoded as red, co-polarized light intensity as green, and the background is attributed to blue (negligible). This RGB mapping creates a composite visualization where combined intensities lead to observed colors. Specifically, when both depolarized (red) and co-polarized (green) light intensities are present in a region, their superposition yields a yellow hue in accordance with the principles of additive color mixing, whereas greenish shades indicate co-polarized backscatter.

Whereas Figure 4A provides a comprehensive visualization of the lidar signal through sequential camera exposures, Figure 4B displays the intensity distribution observed at a single exposure, thereby delineating a particular temporal instance within observation. This observation exhibits a strong signal in co-polarization. It also displays a weaker, albeit significant, depolarized signal. The pixel number covered by a single insect transit, also known as the pixel footprint in Figure 4A, is calibrated to height and apparent size in Figure 4B, where the apparent size provides an estimate of the insect's dimensions, as discussed earlier. The height above ground where the signal was detected was calculated based on the Scheimpflug configuration. In the case of triangulating lidar, the primary source of range inaccuracy comes from the beam width, which typically yields around 3%–5% variation.[37] Figure 4B shows a change in range of 8 m at a height of 128 m. If the object being measured is flying at a constant height in an east-west direction, then this translates to a precision of about 6% (Δ8m/128m). This seems to align well with the expected precision of the lidar system. For this observation, the moth appeared to have a length of 35 mm and was heading downward at a speed of ~1.1 m/s. Figure 4C illustrates the time series of both polarization bands showing the higher-frequency oscillations of the wings

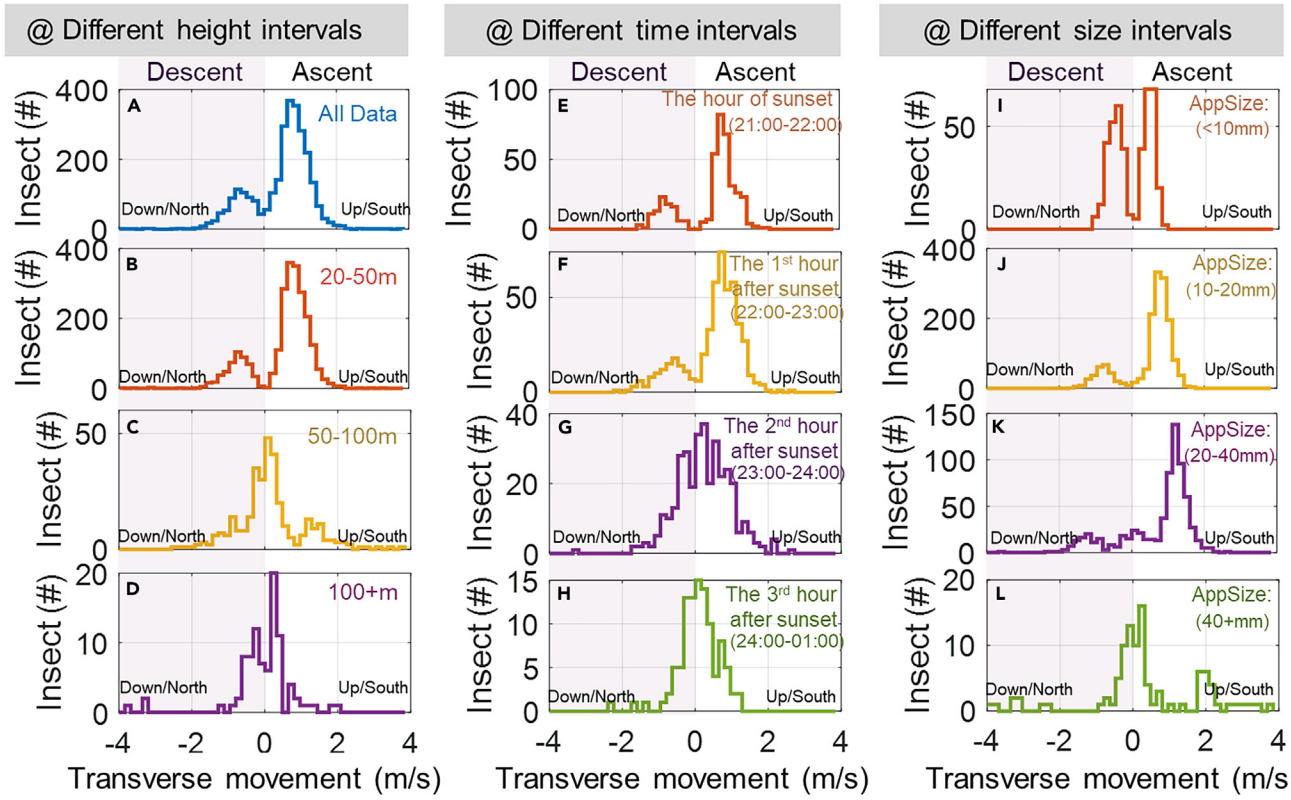

Figure 3. Variation in insect flight direction and speed based on height (A–D), time (A, E–H), and insect size (A, I–L) intervals, all types of insects included

AppSize is short for apparent size. Positive values indicate upward (ascending) flights, while negative values indicate downward (descending) flights.

(A) An overview of the overall distribution observed throughout the entire day and over all heights and sizes.

(A–D) The variation in insect speed and heading at different height intervals summed across the entire day.

(A and E–H) The temporal changes in flight speed and heading direction at specific time intervals following sunset (at ~22:00), all heights included.

(A and I–L) Variances in flight direction and velocity, for different insect size intervals summed across the entire day.

superimposed on a bias envelope arising from the moth's body. With polarimetric information, we can confidently deduce that this signal is from a moth due to its high depolarization in the wing signal; such signals are observed in Lepidoptera (butterflies or moths) with diffuse wings.[27] In contrast, clear-winged insects, such as wasps or hoverflies, display negligible wing depolarization effects due to their ultra-thin wing membranes.[40,41] Figure 4D presents the corresponding power spectrum. The fundamental frequency could only be estimated for the co-polarized signal and was found to be 56 Hz. This low wingbeat frequency is another indicator that this signal originated from a moth.[42–44] Our methodology thus has the potential to allow the differentiation of moths from other insects by leveraging the unique characteristics of wingbeat frequency and polarization. To achieve higher taxonomic precision in our identification process, we foresee the integration of additional wavelengths into our lidar system.[29] Alternatively, the construction of a lookup database with the help of a goniometric polarimetric system,[45] linking specific lidar signals with corresponding moth species, may also prove feasible in the future.

DISCUSSION

Lidar allowed detailed monitoring of the daily activity patterns of insects at low heights (20–200 m) and has also provided robust measures of flying insect density, size, ascents, and descents at different times, heights, and size intervals. This information could be vital for studies of insect migratory behavior since migrations are a large-scale phenomenon, and the impacts of migration (e.g., nutrient flows, herbivory, pollination) are felt locally through emigrations and colonization occurring at low heights. For example, many insects initiate takeoff within 1 h after sunset, exhibiting a nearly equal number of ascents and descents thereafter in our station. This observation suggests that our study area may serve as a population source or transit zone for migratory insects.[39] Moreover, lidar observations, via its successful calculation of apparent size and wingbeat frequency, could allow a deeper and more efficient examination of the individual category and recognization in the future, which is greatly helpful for understanding the adaptions and strategies of small migrants at the low heights.

Since the development of VLR-based tracking methods for diurnal and nocturnal flying vectors,[17,46] a wealth of fascinating phenomena related to insect migration above 150 m have been uncovered.[1,5,13] These discoveries have greatly deepened our understanding of the intricate behavioral patterns (e.g., flight orientations) exhibited by high-flying migratory insects.[1,5] Besides, FMCW radar appears subsequently

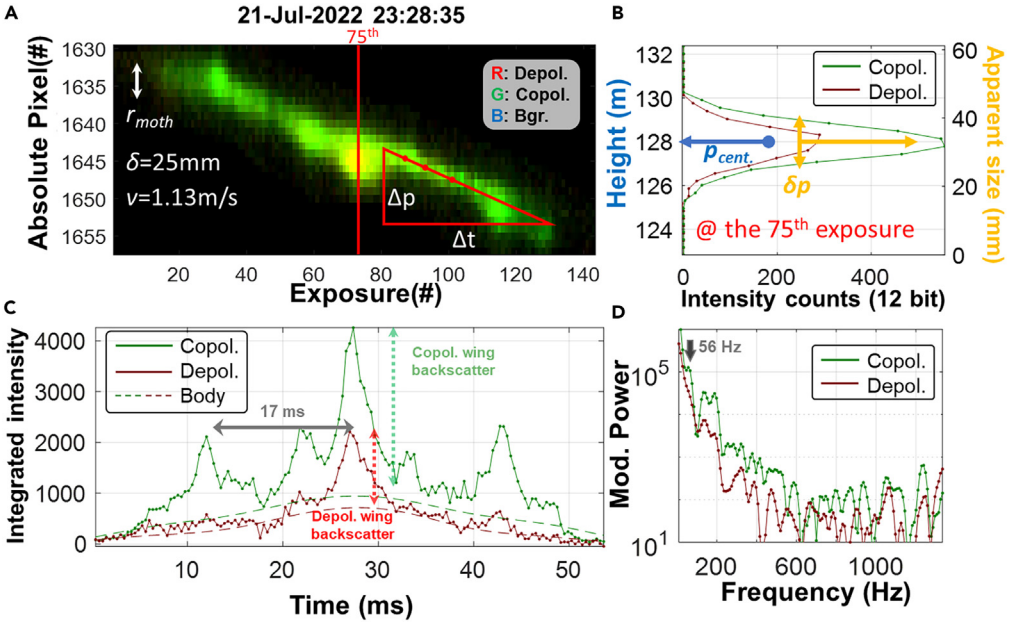

Figure 4. An example of a single moth observation obtained using polarization lidar technology

(A) A spatiotemporal display demonstrating an observation of a single slow oscillatory insect presented as a false color image.

(B) The echo from a single camera exposure of a moth.

(C) Time series of both polarization bands, featuring an oscillatory part from the wing movements and a bias envelope from the insect's body.

(D) Corresponding power spectrum where the fundamental frequency emerges as the highest tone in this specific observation.

with several advancements (lower inherent interference, lower cost, more flexible), to fill the crucial niche of insect migration monitoring below 150 m, which becomes promising remote sensors for tiny migrants nowadays.[20–22] However, the potential of lidar as a complementary technique to VLR or FMCW radar is underappreciated, despite its ability to provide valuable information on horizontal velocities at heights below 200 m. Integrating all of these remote sensors, light traps, and pheromone traps would significantly enhance our ability to unravel the complexities of insect migration and could provide a more complete picture of these dynamics.[1,5]

Although the lidar system has emerged as a complement to radar providing information about the timing, location, size, and wingbeat frequency of individual moths, species classification has proven elusive due to the limitations imposed by the typical beam widths of lidar systems. In this study the average moth transit time measured by the lidar was only around 15 ms, and, for successfully identifying slow-flying moths that have a wingbeat frequency of around 20 Hz, a transit time at least 3 times longer would be required. It is realistic to imagine a dedicated moth-monitoring lidar with an expander providing a 3-times wider beam, although the beam intensity would thereby be diluted by a factor of 9. This is achievable given the laser used in this study was relatively weak, and stronger laser diodes are available at little added cost. In turn, by appropriately changing the beam width, we anticipate that the classification of nocturnal moths can become possible, even at greater heights, from lidars pointed vertically. By using an expanded lidar beam to retrieve optical signals from migrating moths, we would have the potential to classify moth species based on the inherent microstructural differences between them, something that is not possible with VLR. Moreover, other studies have demonstrated the feasibility of remotely classifying moths, further supporting the potential for successful species identification in our research.[27,29,41] Additionally, due to the lidar's near limit, insect activity was not detectable below a range of 20 m, effectively hiding any insect activity within this range. This problem is only worsened by the lidar's narrow beam. These factors also contribute to reducing the likelihood of detecting moths that choose to fly at varying heights or distances from the lidar beam. Another shortcoming of our study is the relatively brief monitoring period we used (18 days), which might have limited our ability to capture longer-term or seasonal behavioral patterns of migratory moths. Future studies can address this issue by establishing a stationary setup and implementing an improved data pipeline, enabling automated and extended collection and analysis of the data.[47]

While we have observed wing depolarization in Lepidoptera, alternative data sources, such as the smooth waveforms in the time domain or sparse harmonics in the frequency domain, could also yield this information. Therefore, exploring alternative technologies, such as a dual-wavelength system, like the one used in Ecuador,[27] could provide more in-depth information. Such systems might prove beneficial considering the differing levels of melanization in the body and wings of Lepidoptera,[29] potentially leading to more detailed observational information.

As we plan the future direction of this research, we believe that our study has established initial signal expectations which now allow us to explore the possibility of developing dedicated systems with increased beam width and power. We are committed to enhancing our understanding of the behavior and ecology of these remarkable nocturnal migrants, and we are confident that future advancements in lidar technology and methodology will continue to play a crucial role in this field.

Limitations of the study

Even though our lidar methods have successfully recorded the flight behaviors of insects, much still needs to be addressed regarding identification of these moths at a species' level. Specifically, our attempts to capture the wing strokes of moths having low wingbeat frequencies was challenging due to the relatively narrow width of the lidar beam. Furthermore, given the oblique angle of the lidar beam, our calculation of apparent vertical velocity of insects, based on transverse velocity, assumes that insect movements are unbiased along the north-south axis. Still, as we plan the future direction of this research, we believe that our study has established initial signal expectations which now allow us to explore the possibility of developing dedicated systems with increased beam width and power in the future.

STAR★METHODS

Detailed methods are provided in the online version of this paper and include the following:

- KEY RESOURCES TABLE
- RESOURCE AVAILABILITY
  - Lead contact
  - Materials availability
  - Data and code availability
- EXPERIMENTAL MODEL AND SUBJECT DETIALS
  - Scheimpflug lidar
  - Laser light multiplexing for polarization data analysis
  - Compensation for observation hours
  - Signal projections on camera chip and movement direction estimation
- QUANTIFICATION AND STATISTICAL ANALYSIS
  - Apparent size calculation
  - Insect velocity calculation

SUPPLEMENTAL INFORMATION

Supplemental information can be found online at https://doi.org/10.1016/j.isci.2024.109588.

ACKNOWLEDGMENTS

This project has received funding from the European Research Council (ERC) under the European Union's Horizon 2020 research and innovation program (grant agreement no. 850463 Bug-Flash and 741298 Magnetic Moth) and from FORMAS the Swedish Research Council (grants 2018-01061 and 2021-04917). We thank Dr. Rachel Muheim (University of Lund), the Director of the Stensoffa Ecological Field Station, for logistical support.

AUTHOR CONTRIBUTIONS

Conceptualization: M.B., E.W., M.L., J.S., P.T., T.T.H. Methodology: M.B., E.W., J.S. Investigation: P.T., J.S., L.M., H.M., M.B., M.L., H.C., D.D., J.A., T.T.H. Visualization: M.B., M.L., H.C. Funding acquisition: M.B., E.W. Project administration: M.B., E.W. Supervision: M.B., E.W. Writing – original draft: H.C., M.L., M.B. Writing – review and editing: H.C., M.L., P.T., J.S., L.M., H.M., D.D., G.H., E.W., M.B., J.A., T.T.H.

DECLARATION OF INTERESTS

The authors declare no competing interests.

Received: September 15, 2023
Revised: January 29, 2024
Accepted: March 25, 2024
Published: March 27, 2024

REFERENCES

1. Hu, G., Lim, K.S., Horvitz, N., Clark, S.J., Reynolds, D.R., Sapir, N., and Chapman, J.W. (2016). Mass seasonal bioflows of high-flying insect migrants. Science *354*, 1584–1587. https://doi.org/10.1126/science.aah4379.
2. Chapman, J.W., Bell, J.R., Burgin, L.E., Reynolds, D.R., Pettersson, L.B., Hill, J.K., Bonsall, M.B., and Thomas, J.A. (2012). Seasonal migration to high latitudes results in major reproductive benefits in an insect. Proc. Natl. Acad. Sci. USA *109*, 14924–14929. https://doi.org/10.1073/pnas.1207255109.
3. Hawkes, W.L.S., Walliker, E., Gao, B., Forster, O., Lacey, K., Doyle, T., Massy, R., Roberts, N.W., Reynolds, D.R., Özden, Ö., et al. (2022). Huge spring migrations of insects from the Middle East to Europe: quantifying the migratory assemblage and ecosystem services. Ecography *2022*. https://doi.org/10.1111/ecog.06288.
4. Wood, C.R., Reynolds, D.R., Wells, P.M., Barlow, J.F., Woiwod, I.P., and Chapman, J.W. (2009). Flight periodicity and the vertical distribution of high-altitude moth migration over southern Britain. Bull. Entomol. Res. *99*,

525–535. https://doi.org/10.1017/S0007485308006548.

5. Chapman, J.W., Reynolds, D.R., Mouritsen, H., Hill, J.K., Riley, J.R., Sivell, D., Smith, A.D., and Woiwod, I.P. (2008). Wind selection and drift compensation optimize migratory pathways in a high-flying moth. Curr. Biol. *18*, 514–518. https://doi.org/10.1016/j.cub.2008.02.080.
6. Alison, J., Alexander, J.M., Diaz Zeugin, N., Dupont, Y.L., Iseli, E., Mann, H.M.R., and Høye, T.T. (2022). Moths complement bumblebee pollination of red clover: a case for day-and-night insect surveillance. Biol. Lett. *18*, 20220187. https://doi.org/10.1098/rsbl.2022.0187.
7. Reynolds, D.R., Chapman, J.W., and Harrington, R. (2006). The migration of insect vectors of plant and animal viruses. Adv. Virus Res. *67*, 453–517. https://doi.org/10.1016/S0065-3527(06)67012-7.
8. Jones, C.M., Parry, H., Tay, W.T., Reynolds, D.R., and Chapman, J.W. (2019). Movement ecology of pest helicoverpa: implications for ongoing spread. Annu. Rev. Entomol. *64*, 277–295. https://doi.org/10.1146/annurev-ento-011118-111959.
9. Riley, J.R., Xia-nian, C., Xiao-xi, Z., Reynolds, D.R., Guo-min, X., Smith, A.D., Ji-yi, C., Ai-dong, B., and Bao-ping, Z. (1991). The long-distance migration of *Nilaparvata lugens* (Stål) (Delphacidae) in China: radar observations of mass return flight in the autumn. Ecol. Entomol. *16*, 471–489. https://doi.org/10.1111/j.1365-2311.1991.tb00240.x.
10. Li, X.J., Wu, M.F., Ma, J., Gao, B.Y., Wu, Q.L., Chen, A.D., Liu, J., Jiang, Y.Y., Zhai, B.P., Early, R., et al. (2020). Prediction of migratory routes of the invasive fall armyworm in eastern China using a trajectory analytical approach. Pest Manag. Sci. *76*, 454–463. https://doi.org/10.1002/ps.5530.
11. Drake, V.A., and Wang, H. (2018). Ascent and descent rates of high-flying insect migrants determined with a non-coherent vertical-beam entomological radar. Int. J. Rem. Sens. *40*, 883–904. https://doi.org/10.1080/01431161.2018.1519283.
12. Drake, V.A., and Wang, H. (2013). Recognition and characterization of migratory movements of Australian plague locusts, *Chortoicetes terminifera*, with an insect monitoring radar. J. Appl. Remote Sens. *7*, 075095. https://doi.org/10.1117/1.Jrs.7.075095.
13. Wotton, K.R., Gao, B., Menz, M.H.M., Morris, R.K.A., Ball, S.G., Lim, K.S., Reynolds, D.R., Hu, G., and Chapman, J.W. (2019). Mass seasonal migrations of hoverflies provide extensive pollination and crop protection services. Curr. Biol. *29*, 2167–2173.e5. https://doi.org/10.1016/j.cub.2019.05.036.
14. Aralimarad, P., Reynolds, A.M., Lim, K.S., Reynolds, D.R., and Chapman, J.W. (2011). Flight altitude selection increases orientation performance in high-flying nocturnal insect migrants. Anim. Behav. *82*, 1221–1225. https://doi.org/10.1016/j.anbehav.2011.09.013.
15. Drake, V.A. (2016). Distinguishing target classes in observations from vertically pointing entomological radars. Int. J. Rem. Sens. *37*, 3811–3835. https://doi.org/10.1080/01431161.2016.1204028.
16. Drake, V.A., Hatty, S., Symons, C., and Wang, H. (2020). Insect monitoring radar: maximizing performance and utility. Remote Sens. Basel *12*, 596. https://doi.org/10.3390/rs12040596.
17. Riley, J.R. (1989). Remote sensing in entomology. Annu. Rev. Entomol. *34*, 247–271. https://doi.org/10.1146/annurev.en.34.010189.001335.
18. Chapman, J.W., Reynolds, D.R., and Smith, A.D. (2003). Vertical-looking radar: a new tool for monitoring high-altitude insect migration. Bioscience *53*, 503–511. https://doi.org/10.1641/0006-3568(2003)053[0503:Vrantf]2.0.Co;2.
19. Feng, H.Q., Zhao, X.C., Wu, X.F., Wu, B., Wu, K.M., Cheng, D.F., and Guo, Y.Y. (2008). Autumn migration of *Mythimna separata* (Lepidoptera: Noctuidae) over the Bohai Sea in Northern China. Environ. Entomol. *37*, 774–781. https://doi.org/10.1093/ee/37.3.774.
20. Noskov, A., Achilles, S., and Bendix, J. (2021). Presence and Biomass Information Extraction from Highly Uncertain Data of an Experimental Low-Range Insect Radar Setup. Diversity *13*, 452. https://doi.org/10.3390/d13090452.
21. Noskov, A., Bendix, J., and Friess, N. (2021). A Review of Insect Monitoring Approaches with Special Reference to Radar Techniques. Sensors *21*, 1474. https://doi.org/10.3390/s21041474.
22. Noskov, A., Achilles, S., and Bendix, J. (2023). Toward forest dynamics' systematic knowledge: concept study of a multi-sensor visually tracked rover including a new insect radar for high-accuracy robotic monitoring. Front. Ecol. Evol. *11*. https://doi.org/10.3389/fevo.2023.1214419.
23. Brydegaard, M., and Svanberg, S. (2018). Photonic monitoring of atmospheric and aquatic fauna. Laser Photon. Rev. *12*, 1800135. https://doi.org/10.1002/lpor.201800135.
24. Månefjord, H., Müller, L., Li, M., Salvador, J., Blomqvist, S., Runemark, A., Kirkeby, C., Ignell, R., Bood, J., and Brydegaard, M. (2022). 3D-Printed fluorescence hyperspectral lidar for monitoring tagged insects. IEEE J. Sel. Top. Quant. *28*, 1–9. https://doi.org/10.1109/JSTQE.2022.3162417.
25. Song, Z., Zhang, B., Feng, H., Zhu, S., Hu, L., Brydegaard, M., Li, Y., Jansson, S., Malmqvist, E., Svanberg, K., et al. (2020). Application of lidar remote sensing of insects in agricultural entomology on the Chinese scene. J. Appl. Entomol. *144*, 161–169. https://doi.org/10.1111/jen.12714.
26. Jansson, S., Malmqvist, E., Mlacha, Y., Ignell, R., Okumu, F., Killeen, G., Kirkeby, C., and Brydegaard, M. (2021). Real-time dispersal of malaria vectors in rural Africa monitored with lidar. PLoS One *16*, e0247803. https://doi.org/10.1371/journal.pone.0247803.
27. Santos, V., Costa-Vera, C., Rivera-Parra, P., Burneo, S., Molina, J., Encalada, D., Salvador, J., and Brydegaard, M. (2023). Dual-band infrared Scheimpflug lidar reveals insect activity in a tropical cloud forest. Appl. Spectrosc. *77*, 593–602. https://doi.org/10.1177/00037028231169302.
28. Li, M., Jansson, S., Runemark, A., Peterson, J., Kirkeby, C.T., Jönsson, A.M., and Brydegaard, M. (2021). Bark beetles as lidar targets and prospects of photonic surveillance. J. Biophot. *14*, e202000420. https://doi.org/10.1002/jbio.202000420.
29. Li, M., Seinsche, C., Jansson, S., Hernandez, J., Rota, J., Warrant, E., and Brydegaard, M. (2022). Potential for identification of wild night-flying moths by remote infrared microscopy. J. R. Soc. Interface *19*, 20220256. https://doi.org/10.1098/rsif.2022.0256.
30. Li, M., Runemark, A., Hernandez, J., Rota, J., Bygebjerg, R., and Brydegaard, M. (2023). Discrimination of hover fly species and sexes by wing interference signals. Adv. Sci. *10*. https://doi.org/10.1002/advs.202370232.
31. Li, Y.Y., Zhang, H., Duan, Z., Lian, M., Zhao, G.Y., Sun, X.H., Hu, J.D., Gao, L.N., Feng, H.Q., and Svanberg, S. (2016). Optical characterization of agricultural pest insects: a methodological study in the spectral and time domains. Appl. Phys. B *122*, 213. https://doi.org/10.1007/s00340-016-6485-x.
32. Brydegaard, M., Kouakou, B., Jansson, S., Rydell, J., and Zoueu, J. (2021). High dynamic range in entomological scheimpflug lidars. IEEE J. Sel. Top. Quant *27*, 1–11. https://doi.org/10.1109/JSTQE.2021.3062088.
33. Rydhmer, K., Prangsma, J., Brydegaard, M., Smith, H.G., Kirkeby, C., Kappel Schmidt, I., and Boelt, B. (2022). Scheimpflug lidar range profiling of bee activity patterns and spatial distributions. Anim. Biotelemetry *10*, 14. https://doi.org/10.1186/s40317-022-00285-z.
34. Brydegaard, M., Jansson, S., Malmqvist, E., Mlacha, Y.P., Gebru, A., Okumu, F., Killeen, G.F., and Kirkeby, C. (2020). Lidar reveals activity anomaly of malaria vectors during pan-African eclipse. Sci. Adv. *6*, eaay5487. https://doi.org/10.1126/sciadv.aay5487.
35. Wiktelius, S. (1984). Long range migration of aphids into Sweden. Int. J. Biometeorol. *28*, 185–200. https://doi.org/10.1007/BF02187959.
36. Li, Y., Wang, K., Quintero-Torres, R., Brick, R., Sokolov, A.V., and Scully, M.O. (2020). Insect flight velocity measurement with a CW near-IR Scheimpflug lidar system. Opt Express *28*, 21891–21902. https://doi.org/10.1364/OE.394992.
37. Malmqvist, E., Brydegaard, M., Aldén, M., and Bood, J. (2018). Scheimpflug Lidar for combustion diagnostics. Opt Express *26*, 14842–14858. https://doi.org/10.1364/OE.26.014842.
38. Jansson, S., and Brydegaard, M. (2018). Passive kHz lidar for the quantification of insect activity and dispersal. Anim. Biotelemetry *6*, 6. https://doi.org/10.1186/s40317-018-0151-5.
39. Rydhmer, K., Jansson, S., Still, L., Beck, B.D., Chatzaki, V., Olsen, K., Van Hoff, B., Grønne, C., Meier, J.K., Montoro, M., et al. (2024). Photonic sensors reflect variation in insect abundance and diversity across habitats. Ecol. Indicat. *158*, 111483. https://doi.org/10.1016/j.ecolind.2023.111483.
40. Müller, L., Li, M., Månefjord, H., Salvador, J., Reistad, N., Hernandez, J., Kirkeby, C., Runemark, A., and Brydegaard, M. (2023). Remote nanoscopy with infrared elastic hyperspectral lidar. Adv. Sci. *10*, 2207110. https://doi.org/10.1002/advs.202207110.
41. Li, M., Runemark, A., Guilcher, N., Hernandez, J., Rota, J., and Brydegaard, M. (2023). Feasibility of insect identification based on spectral fringes produced by clear wings. IEEE J. Sel. Top. Quant. *29*, 1–8. https://doi.org/10.1109/JSTQE.2022.3218218.
42. Willmott, A.P., and Ellington, C.P. (1997). The mechanics of flight in the hawkmoth *Manduca sexta*. I. Kinematics of hovering and forward flight. J. Exp. Biol. *200*, 2705–2722. https://doi.org/10.1242/jeb.200.21.2705.
43. Warfvinge, K., Johansson, L.C., and Hedenström, A. (2021). Hovering flight in hummingbird hawkmoths: kinematics, wake dynamics and aerodynamic power. J. Exp. Biol. *224*, jeb230920. https://doi.org/10.1242/jeb.230920.

44. Huang, J.l., Qiu, M., and Ma, L.l. (2013). Effects of age, ambient temperature and reproductive status on wing beat frequency of the rice leafroller *Cnaphalocrocis medinalis* (Guenée) (Lepidoptera: Crambidae). Appl. Entomol. Zool. *45*, 499–503. https://doi.org/10.1007/s13355-013-0209-z.

45. Månefjord, H., Li, M., Brackmann, C., Reistad, N., Runemark, A., Rota, J., Anderson, B., Zoueu, J.T., Merdasa, A., and Brydegaard, M. (2022). A biophotonic platform for quantitative analysis in the spatial, spectral, polarimetric, and goniometric domains. Rev. Sci. Instrum. *93*, 113709. https://doi.org/10.1063/5.0095133.

46. Dwivedi, M., Shadab, M.H., and Santosh, V.R. (2020). Insect pest detection, migration and monitoring using radar and LiDAR systems. In Innovative Pest Management Approaches for the 21st Century: Harnessing Automated Unmanned Technologies, pp. 61–76. https://doi.org/10.1007/978-981-15-0794-6_4.

47. Lukach, M., Dally, T., Evans, W., Hassall, C., Duncan, E.J., Bennett, L., Addison, F.I., Kunin, W.E., Chapman, J.W., and Neely, R.R., 3rd (2022). The development of an unsupervised hierarchical clustering analysis of dual-polarization weather surveillance radar observations to assess nocturnal insect abundance and diversity. Remote Sens. Ecol. Conserv. *8*, 698–716. https://doi.org/10.1002/rse2.270.

48. Jansson, S., Malmqvist, E., Brydegaard, M., Åkesson, S., and Rydell, J. (2020). A Scheimpflug lidar used to observe insect swarming at a wind turbine. Ecol. Indicat. *117*, 106578. https://doi.org/10.1016/j.ecolind.2020.106578.

49. Kouakou, B.K., Jansson, S., Brydegaard, M., and Zoueu, J.T. (2020). Entomological Scheimpflug lidar for estimating unique insect classes in-situ field test from Ivory Coast. OSA Continuum *3*, 2362. https://doi.org/10.1364/osac.387727.

50. Spie, P.o., Malmqvist, E., Jansson, S., Larsson, J., Török, S., and Zhao, G. (2017). The Scheimpflug lidar method. Lidar Remote Sensing for Environmental Monitoring *10406*, 104060I. https://doi.org/10.1117/12.2295982.

51. Mei, L., and Guan, P. (2017). Development of an atmospheric polarization Scheimpflug lidar system based on a time-division multiplexing scheme. Opt. Lett. *42*, 3562–3565. https://doi.org/10.1364/OL.42.003562.

52. Zhao, G., Malmqvist, E., Török, S., Bengtsson, P.-E., Svanberg, S., Bood, J., and Brydegaard, M. (2018). Particle profiling and classification by a dual-band continuous-wave lidar system. Appl. Opt. *57*, 10164–10171. https://doi.org/10.1364/AO.57.010164.

53. Jansson, S. (2020). Entomological lidar: target characterization and field applications. PhD Thesis (Lund University). https://lup.lub.lu.se/search/publication/0a1b0d54-552d-4a3f-805a-c848932d1de2.

STAR★METHODS

KEY RESOURCES TABLE

REAGENT or RESOURCE	SOURCE	IDENTIFIER
Deposited data		
Raw data files	Meng Li, Mikkel Brydegaard, Lund University, Sweden	https://lu.box.com/s/c7a1jxneh8owxuyh0r725ocbzi0bjcqh
Analyzed data files	This paper	Figures 1, 2, 3, and 4
Software and algorithms		
LabVIEW 2022	National Instruments	https://www.ni.com/en/support/downloads.html
Custom made LabView code for Scheimpflug Lidar data acquisition	This paper; Hampus Månefjord, Lund University, Sweden	https://github.com/BioBeamMeng/LidarMoth
MATLAB 2022	MathWorks	https://se.mathworks.com/
Custom Matlab-script was used for data and figure analysis	This paper; Meng Li, Mikkel Brydegaard, Lund University, Sweden	https://github.com/BioBeamMeng/LidarMoth

RESOURCE AVAILABILITY

Lead contact

Further information and requests for resources should be directed to and will be fulfilled by the Lead Contact, Mikkel Brydegaard (mikkel.brydegaard@fysik.lth.se).

Materials availability

This study did not generate new unique reagents.

Data and code availability

- All data reported in this paper have been deposited at GitHub, and are publicly available as of the date of publication, as detailed in the key resources table.
- This paper does not report original code.
- Any additional information required to reanalyze the data reported in this paper is available form the lead contact upon request.

EXPERIMENTAL MODEL AND SUBJECT DETIALS

Scheimpflug lidar

Our lidar system was based on the Scheimpflug lidar principle,[26–28,32,48,49] which allows us to focus on flying insects over varying distances simultaneously. This lidar system is mounted on an 814 mm long baseline with a transmitting and a receiving telescope, as depicted in Figure 1A. For stabilization, we utilized a tripod (EQ8, SkyWatcher, China).

The transmitting telescope, integrated with two 3W TE-polarized 980 nm laser diodes, has an aperture of 75 mm and a focal length of 300 mm. The 980 nm wavelength is near-infrared, invisible and do not disturb air traffic. Eye-safe levels were obtained beyond 30 m range and 15 m altitude. The beam is inaccessible. The polarization from one laser diode is altered by 90° using a wide-angle polymer half-wave plate and superimposed with the other laser beam via a polarization beam splitter, then transmitted.

The receiving telescope is a Ø200 mm, f800 mm Newton reflector (Quattro, SkyWatcher, China) equipped with a CMOS detector (OctoPlus, Teledyne e2v, USA) at its eyepiece to collect signal data. This CMOS detector consists of 2048 pixels, each measuring 10 μm × 200 μm. In line with the Scheimpflug principle and the hinge rule,[49,50] the camera is tilted at a 45° angle relative to the optical axis within the transmitter module.

The lidar system, employing a polarimetric configuration, operated at an 8 kHz sampling rate, with co-polarized, de-polarized, and background signals being sampled at approximately 2.66 kHz each after de-multiplexing.[51,52] Each lidar file contained a 4-s length of observation data with 30,000 exposure lines. Each file was around 120 MB in size, and throughout the campaign, more than 20 TB of raw data was acquired. In the process of data acquisition, the polarization of the laser light was multiplexed, allowing for the sequential capture of depolarized,

co-polarized, and background light. Subsequent processing steps involved the subtraction of the depolarized, co-polarized, and background signals from the raw data, and cropping out the insect observation signal following the data processing pipeline.[53] As most of the data were empty, the data size was reduced to less than 1% of the original size. In total, we acquired lidar signals for 18 days. Operating at a fast-sampling rate of 8 kHz (equivalent to a short exposure time of 125 μs), our lidar system efficiently distinguishes insect signals from atmospheric particles and aerosols with a threshold SNR of 5. Typically, achieving a reliable signal from air particles or aerosols would necessitate longer exposure times. For example, capturing air signals would require an exposure setting of 620 μs, in addition to doubling the gain and preamplification when using our lidar system.

The typical cost for the construction of these lidar systems ranges from 15 to 20 kEuro, which includes travel boxes, and other associated expenses. A dozen systems have been assembled within this budget. The timeline for this process involves three months for ordering components and assembling the system, followed by an additional three months for alignment and mastering the analysis code.

Laser light multiplexing for polarization data analysis

For a comprehensive view of each measurement day, we generate overview plots (like the example shown in Figure S1). These plots color-code the maximum depolarized, copolarized, and background values within each file. This visualization reveals temporal and spatial shifts in maximum values and emphasizes rare events (e.g., insects appear as bright green dots). Cloud echoes are also evident, with higher atmospheric scatter coefficients and humidity causing clouds to descend during evening hours.

To demonstrate how we use a threshold to pick out insect observations, frame 3991 (recorded at 06-Jun-2022 22:46:08 and marked in Figure S1A) is examined. Figure S1B zooms in on this time frame, highlighting distinct signals (later classified as insects) alongside persistent aerosol plumes (clouds). Intensity counts for frame 3991, including pixel-wise median and maximum values, are shown in Figure S1C. A threshold based on each pixel's intensity distribution isolates insect signals from aerosols (e.g., clouds). This threshold is the median plus five times the interquartile range (IQR), or SNR = 5. The SNR ratio is configurable; we employed SNR = 5 to visually confirm the threshold appropriately suppressed cloud/mist signals while preserving insects. Higher or lower SNRs may be suitable depending on observational conditions (e.g., dense fog). Figure S1D illustrates how the threshold varies with a pixel's median and IQR; the insect pixel retains some values above the threshold, while all cloud pixel values are eliminated due to its broader IQR and higher median. This demonstrates the threshold's (Figure S1C) effectiveness in selecting rare events (insects, with lower median and IQR) over continuous aerosol signals.

During the data acquisition process, the laser light was multiplexed, enabling it to sequentially illuminate in depolarized, co-polarized, and background modes. This multiplexing sequence is represented in Figures S2A and S1B, where the strips of signals in the captured data change as the laser light transitions between its modes. After acquisition, the background signals were subtracted from both the co-polarized and depolarized signals, as depicted in Figures S2C and S1D. To distinguish insect signals from background noise, a threshold was applied, with Figure S2E showing the use of a detection mask that retains only those signals exceeding an SNR of 5. Further procedures to isolate and crop the insect signals are described in detail in previous study.[53]

Compensation for observation hours

As mentioned earlier, the lidar system was not operated continuously, resulting in a bias in the observations. There were more observations recorded between 18:00 and 24:00 compared to full-day recordings, leading to a false insect activity pattern as shown in Figure S3A. In Figure S3B, it is evident that there is a higher accumulation of files recorded during the 18:00 to 24:00 time period, indicating the bias caused by the uneven lidar operation hours. To address this bias, the insect activity pattern was compensated using Figure S3B, resulting in Figure S3C, which removes the effect of lidar operation hours. With the compensation, a higher insect activity is now reported during the daytime as well, but overall, there is still a greater insect activity observed during the evening at higher heights.

Signal projections on camera chip and movement direction estimation

Expounding upon the technique of insect signal detection, an extended illustration from Figure 1C is provided in Figure S4A. Initially, the lidar is set at an elevation angle of 30°, with the beam and the receiver's field of view converging around a distance of 35 m afar (20 m in height). Given the orientation of the camera chip, pixel number p_{2048} captures the observational scene at an elevation angle $\Phi = 30^{\circ}$, whereas pixel p_1 captures at an elevation angle $\Phi + \varphi$, with $\varphi = 1.27^{\circ}$.

Delving into the dynamics of signal detection, the range is ascertained using Equation 3, considering the absolute center pixel location, p_{cent}. For instance, in the scenario depicted in Figure S4B, p_{cent} would be p_{1641} at time t_0 and at time t_1, the signal is captured onto pixel p_{1642}. The traversed distance by the center pixel, denoted as Δp is the signal displacement. By dividing Δp by the time difference Δt, the velocity is then calculated. Additionally, in Figure S4B, the spread of the signal on the chip is denoted as δp. The apparent size can be calculated utilizing the magnification from the camera and telescope, which in turn, is employed to approximate the insect size.

With the Lidar system positioned facing north at an elevation angle of 30°, a positive velocity value, as derived from Equation 2, denotes movement either upwards or toward the south. Figure S4B illustrates the relative camera chip positioning in accordance to the north, south, upward, and downward directions. The differential $\Delta p/\Delta t$, contingent on the value of Δp, registers as positive only when the detected target's movement is directed either upwards or southward. Given the configuration of the Lidar system, it exhibits a greater efficacy in capturing movements directed upwards compared to those directed southward.

QUANTIFICATION AND STATISTICAL ANALYSIS

Apparent size calculation

To determine the apparent size of the insects, symbolized as δ_{insect}, we implemented a formula based on the methodology from a previous study which also used the Scheimpflug lidar configuration,[32]

$$\delta_{\text{insect }(t)} = 4\sqrt{2\log(2)}\,\frac{r\cos(\theta)\,W}{F_{rec}}\sqrt{\frac{\sum_{\text{mask}} I_{\text{insect }(p,t)}\left(p - p_{\text{cent.}}\right)^2}{\sum_{\text{mask}} I_{\text{insect }(p,t)}}} \quad \text{(Equation 1)}$$

where r is the range to the observed insect, W is pixel pitch, the distance from the center of one pixel to the center of the next on the camera, which was 10 μm/pix, θ is the tilt angle of the sensor in the Scheimpflug configuration, set at 45° between the camera and optical axis within the transmitter module. F_{rec} is the focal length of the receiver, which was 0.8 m. The central pixel in our analysis, symbolized as p_{cent}, is calculated using the first statistical moment or the Center of Mass (CoM) calculation. I represents the lidar intensity count as a function of pixels, p, and time, t. The term *mask* denotes the pixels and exposures that exceed a noise level. The right hand square-root term is the second statistical moment (standard deviation) of the range echo to gauge the pixel spread. The left hand scalar term $4(2\log(2))^{½}$ translates the standard deviation into twice the full-with-half-max (FWHM), whereby the value better reflects the whole physical extension of the insect size. Note that the FWHM term is not present in our previous study.[32] All statistical analysis and graphical plotting were conducted in MATLAB R2021a.

Insect velocity calculation

To measure the vertical heading velocity of the insects observed, we employed a formula derived from a previous study.[36] In Scheimpflug lidar, ranging is accomplished by triangulation and thus the range accuracy is limited by the beam width. This uncertainly can be exploited for estimating target sizes[32] and movements perpendicular to the beam.[36] Insect transverse velocity was calculated as

$$v_{\text{up}\,/\,\text{south}} = \frac{F_{\text{rec}}\,W\,\frac{\Delta p}{\Delta t}\cos(\theta)}{r} \quad \text{(Equation 2)}$$

where v (m/s) represents the velocity component of the insect as it moves perpendicular to the optical path of the receiving telescope, a positive value meaning upwards/south (ascending) flight and a negative value meaning downwards (descending) flight. $\Delta p/\Delta t$ (pix/s) is the number of pixels per unit time, which is itself obtained from a linear fit of the insect signal trajectory in a time-pixel map. Finally, F_{rec} and r refer to the object and image distances, respectively, with the relationship between these two factors specifying the specific magnification for pixel x. W and θ are constants set to 10 μm/pix and 45°, respectively. The estimated range r is calculated by

$$\hat{r}(p_r) = \ell_{\text{BL}}\cot\left(\Gamma_{\text{slant}} + \varphi p_{cent}\right) \quad \text{(Equation 3)}$$

The normalized pixel positions are represented by p_r which range from 0 to 1. ℓ_{BL} denotes the baseline length, set at 0.814 m Γ_{slant} is the angle between the optical axis of the beam expander and the receiver. The receiver's field of view is given by φ. The center pixel, p_{cent}, is determined using the center of mass formula, or CoM. All statistical analysis and graphical plotting were conducted in MATLAB R2021a.